IIETA International Information and Engineering Technology Association
Advancing the World of Information and Engineering

Journal Européen des Systèmes Automatisés
Vol. 59, No. 8, August, 2026, pp. 2273-2289
Journal homepage: http://iieta.org/journals/jesa

Microstructural Differences in Dissimilar Aluminum Alloys Welded by Friction Stir Welding

Luqman Khaleel Hyder Alatrushi[1], Yasir Hassan Ali[1], Zainab Qusay Shareef[1], Emad Toma Karash[2*], Hasan Mahmood Kaedhi[1], Ahmed Mohammed Mahmood[2], Jamal Nayief Sultan[2]

[1] Department of Mechanical Engineering Techniques, Polytechnic College Mosul, Northern Technical University, Mosul 41001, Iraq
[2] Fuel and Energy Engineering Department, AL-Amarah University, Amarah 62001, Iraq

Corresponding Author Email: emad.tomabane.karash@alamarahuc.edu.iq

Copyright: ©2026 The authors. This article is published by IIETA and is licensed under the CC BY 4.0 license (http://creativecommons.org/licenses/by/4.0/).

https://doi.org/10.18280/jesa.590814

Received: 1 June 2026
Revised: 10 August 2026
Accepted: 19 August 2026
Available online: 31 August 2026

Keywords:
compression, microstructure, hardness, friction stir welding, AA-2024-O, AA-7075-T6, deformation

ABSTRACT

Solid-state welding techniques, such as friction stir welding (FSW), are widely used to permanently join metal components without melting them. This is achieved by utilizing the heat generated by friction and elastic deformation to form a strong bond between the materials. This technique is of paramount importance for aluminum alloys, where precise microstructure control plays a crucial role in achieving good mechanical properties. During the welding process, distinct thermal zones are formed, each possessing its own unique structural characteristics due to temperature variations and material flow. This study aims to investigate the effect of welding parameters, especially rotational speed and linear motion speed, on the microstructure and toughness of two different aluminum alloys, AA7075-O and AA2024-T6. To achieve this objective, three distinct zones in the weld area were selected and analyzed using an optical microscope to observe any changes in their structure and evaluate their effects at the mechanical level in terms of hardness and grain size. The study demonstrated that the particle size is precise and homogeneous, which enhances the controlled toughness and strength of the weld joints when using FSW. Microscopic examination revealed that particle size in the mixing zone increases with increasing welding pen speed while maintaining a constant feed cart speed. Conversely, increasing the feed cart speed while keeping the welding pen speed constant results in a decrease in particle size in the mixing zone. Furthermore, increasing the feed rate leads to increased brittleness of the second-phase particles in the mixing zone, resulting in a decrease in hardness.

1. INTRODUCTION

Friction stir welding (FSW) is currently extensively practiced in the automobile and aerospace industries, among others. FSW was invented and patented by the Welding Institute of the UK in 1990 for the welding of plates in a solid state [1]. FSW is an ideal welding process to use for aircraft fuel tanks [2, 3]. Friction stir welds were shown to be comparable to and occasionally even superior to riveted connections after successful static and dynamic testing [3-5]. According to the study's results, welded joints exhibit same corrosion resistance that is comparable to the corrosion resistance of the original material models in the stirring area, which is caused by friction during the FSW process [6]. During welding, the base metal (BM) undergoes significant plastic and heat deformation depending on the degree of thermo-mechanical coupling, producing four unique areas across the joint cross-section: The stir zone, the thermo-mechanically affected region, the heat-affected region, and the BM [7, 8]. As a result, there would be variations in the mechanical characteristics and corrosion behavior within these different zones; this is especially for welded joints of dissimilar metal pieces [9, 10]. After the welding and heating processes are complete, the sheets are moved. Due to friction between the welding tool and the plates' upper surface, the welding tool heats the plates to the point of softening them. It also works to move the metal by mixing as a result of the rotational movement of the welding tool and the support, which causes plastic deformation. As a result, the seam will be joined. Metal mixing and plastic deformation at high temperatures produce a small-grained microstructure with equal axes [11-13]. According to several microhardness measurements [14], the heat-affected region has a substantially lower hardness than the surrounding material. FSW is a wonderful approach to utilize both of the two aluminum alloys because they each have unique features. According to the study [15], the microstructural properties and tensile performance of friction stir welded joints made from the two dissimilar aluminum alloys were studied. The study [16] used the FSW method to examine the mechanical strength and structural makeup of different aluminum welds. According to their investigation, when the aluminum grain size reduced from the top to the middle, the SiC particle size did not change significantly. In Study [17], movement speeds

ranging from 25 to 300 mm/min and tool rotation speeds of 800 and 1250 rpm were used. The microstructure, mechanical properties, and fracture surfaces of the joints were investigated. The results showed optimal welding forces of 396 and 360 MPa were achieved in underwater and air-cooled welds at tool rotation speeds of 800 rpm and movement speeds of 50 mm/min. The research [18] involved the frictional welding of AA 3003 aluminum alloys with different primary microstructures under various welding conditions. The evolution of the microstructure and mechanical properties of the weld joints was studied. The results obtained from this study showed that the recrystallized grain size and the amount of second-phase particles in the weld zone (WNZ) decrease with decreasing ambient welding temperature. The study [19] was done to find out the influence of weld shoulder shapes on grain microstructure and crystalline texture formation in the center interface zone (CIZ) and bottom interface zone (BIZ) of AA2024/AA7075 joints by means of quantitative electron backscattered diffraction. Based on the results obtained, there is a considerable presence of coarse and fine grains of an axial structure in the CIZ and BIZ of joints produced with concentric circle shoulder (CCS) and three-helix shoulder (THS). Also, it was observed that the grain sizes in the BIZ were smaller than those of the CIZ of the same joint formed through CCS and THS. The study [20] proved that most weld joints on the side containing the aluminum alloy (AA2024) failed in the heat-affected zone (HAZ) region, while a few failed in the melt zone. Furthermore, it was found that the elongation and overall strength of the welded joints were lower than those of the original alloys without the use of welding technology. The microstructure and mechanical characteristics of butt joints made from two different aluminum alloys and friction-welded were examined in study [21]. With increasing tool rotation speed, a rise in joint strength was seen in the tensile strength test. The models utilized on the aluminum alloy (6061) side frequently failed and broke. FSW was used to join two different aluminum alloys together [22]. The moving side has the aluminum ingot (7075), while the retreating side has the aluminum alloy (5083). Additionally, a neural network and an algorithm were employed to enhance the welding process's mechanical characteristics, internal structure, and grain size regulation.

The mechanical characteristics and microstructure of 5083-7B04 welds were described by the study [23]. Three different heat treatment methods artificial aging, natural aging, and annealing were used in this investigation on the 7B04 alloy. The joint between the artificially aged 7B04 alloy and the 5083 alloy placed on the advancing side exhibited the best material mixing behavior and mechanical performance, with a tensile strength of 525 MPa. Study [24] investigated how process variables, including rotational and travel speeds, affect the macrostructure, microhardness, and mechanical properties of FSW butt joints fabricated from dissimilar materials. The macroscopic observations showed the stir zone to have different forms and flaws brought on by both too much and not enough heat input. Aerospace aluminum alloys that are challenging to weld can be joined using the clean welding technique of FSW. The friction stir welded joints' tensile characteristics, microhardness, microstructure, and fracture surfaces were examined. At the stir zone, grain refinement is seen as a result of dynamic recrystallization brought on by extreme plastic deformation. The minimum strength for a dissimilar joint metal is seen mostly as a result of the base materials' inhomogeneous movement as a result of variations in their mechanical and physical properties [25]. Numerous studies have examined various FSW parameters, including altering the welding cart's linear speed, the feeding pen rotational speed, and various metal types, particularly aluminum alloys. Studies [26-33] aimed to enhance the internal composition and mechanical characteristics of the welded objects. The researchers may get different FSW links from alloys in the 2xxx and 7xxx families, according to previously published works. In order to determine whether it is possible to accelerate the welding process by increasing welding tool speed without compromising the joint's strength characteristics, a study is still being done on the impact of welding process factors on the attributes of these junctions. In addition, the heat input ratio can be used to evaluate the combined impact of the FSW factors. Since solid connections between alloys (AA-2024-O and AA-7075-T6) with appropriate mechanical properties are desired, this study aims to understand the internal structure of the weld zone and its surrounding areas.

In this paper, the impact of varying the linear speed of the welding tool and the feed on the microstructure of two dissimilar aluminum alloys will be examined. The FSW method will be used to choose various regions of the two welded alloys' surfaces to study. Because the temperatures brought on by the friction process are not equal, these places are situated at the start of the welding time, halfway of the welding process, and at the end of the welding time; this allows us to determine the difference in the internal composition.

2. EXPERIMENTAL WORK

2.1 Materials and techniques

Two different alloys were prepared (sheets of heat-treated aluminum alloys (AA2024-O and AA7075-T6). Each had nine models, each model had dimensions of (100 × 100 × 6 mm), by using FSW. The welding tools were rotated at various speeds (1000, 1250, and 1525 rpm), and various speeds for welding feed (20, 40, 600 mm/min). The chemical composition of several aluminum alloys is shown in study [26], together with the values of the international standard d ratios adopted by the European Aluminum Association (EAA). The cutting pin tool's rotational speed and the feed's linear speed for each of the nine variants are shown in Table 1. The welding tool used in this study was cylindrical, 18.25 mm in diameter, and made of high-speed steel. It had a conical tip with a base diameter of 5.75 mm, a pointed tip of 4.75 mm, and a height of 2.95 mm, which represents plunge depth. The welding angle 2.25° of the welding tool from the vertical axis was chosen because it yielded the best welds in practical experiments conducted by varying the tool's angle of inclination. The tool rotated clockwise during welding, and the material on the advancing side was AA2024-O. Vickers hardness was measured according to ASTM E384 using a Zwick typ./Roell Z HVVickers's with a load of 400 gm and dwell time of 15 s. Measurements were taken in the BM, HAZ, TMAZ, and WNZ, with repeated readings at each location. Grain size was measured according to ASTM E112 using the line-intercept method and calibrated optical microscopy.

2.2 Examination areas

The welded pieces were examined microscopically at different locations, namely at the beginning of the weld process, midway, and in the weld end area. Seven points were taken in each region, and Figure 1 shows these regions in detail.

Table 1. Welding parameters for the nine experimental groups

No.	Group Number	Rotational Speed (rpm)	Linear Speed (mm/min)
1	First	1000	20
2	Second		40
3	Third		60
4	Fourth	1250	20
5	Fifth		40
6	Sixth		60
7	Seventh	1525	30
8	Eighth		40
9	Ninth		60

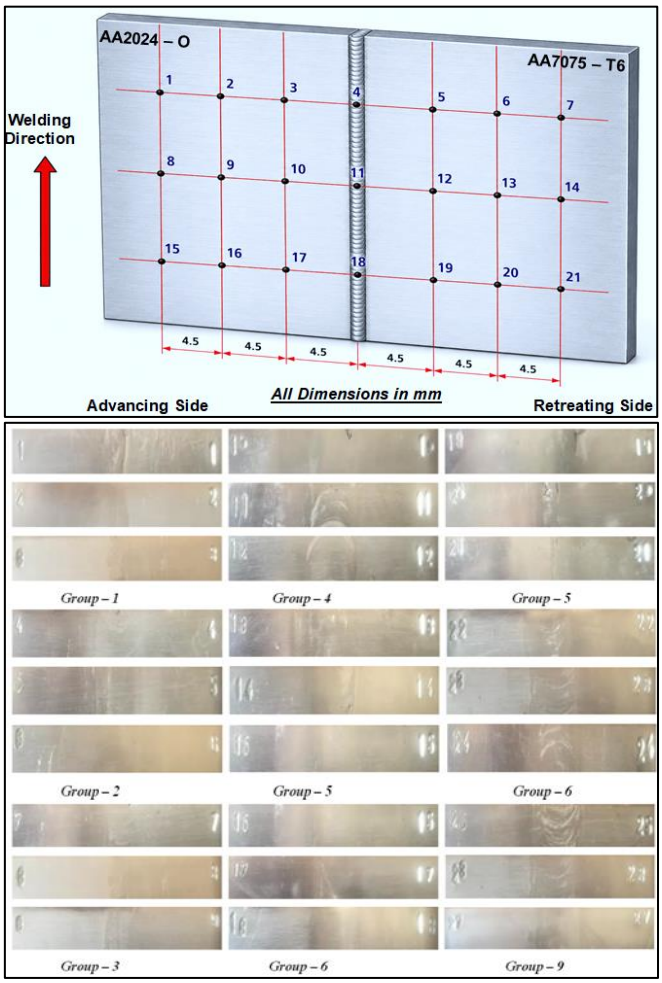


Figure 1. The locations where the welded pieces' microstructure was investigated

2.3 Method of work and examination

The following procedures were followed in order to conduct a microscopic investigation of the samples on which the FSW process was applied:

1. In order to make sure that each group appropriately depicts the circumstances in which the FSW procedure was applied to the samples, the samples to be conducted for the microscopic inspection were cut into dimensions (75 × 30 × 6 mm) and distributed in the form of groups.

2. To get rid of dirt and contaminants, specific detergents were used to clean the surfaces of the samples.

3. The sample surfaces were ground and polished with water. The following polishing papers were used: 200, 400, 600, 1500, 2000, and 3000. The polishing procedure was carried out by orthogonally shifting the samples' axes, and as a result, a smooth surface suited for the display process was produced.

4. Using a rotating tool and a softening solution (Al_2O_3), the surfaces of the test samples were smoothed.

5. The surfaces were cleaned by spraying with water.

6. The chemical composition of the etching solution used for aluminum alloy visualization is presented in Table 2. Each sample was exposed to the solution for 10 to 15 seconds, following which it was washed off and the samples were prepared for microscopic analysis.

7. An electron microscope with a power of 600 was used for microscopy, while a camera with a power of 50MB was used to take photographs.

Table 2. Chemical composition of the etching solution used for aluminum alloy visualization

Substance	Quantity	Unit
Acetic aced	20	ml
Water	15	ml
Picric acid	15	gr
Ethanol (95%)	100	ml

3. RESULTS AND DISCUSSION

3.1 Microstructure

An optical powered light microscope (X600) was used to examine all models after they had been configured for this examination. The areas of the samples' microstructure that were studied are depicted in Figure 1. The first group represents points 1, 2, 3, 4, 5, 6, and 7; the second group represents points 8, 9, 10, 11, 12, and 13; and the third group represents points 15, 16, 17, 18, 19, and 20, respectively. Each sample was separated into three groups. Figure 1 also shows the different regions, which are the HAZ on the advancing side represented by the points (1, 8, 15), the affected zone TMAZ on the advancing side (2, 9, 16), the stir zone (SZ) region represented by the points (3, 4, 5, 10, 11, 12, 17, 18, 19), and TMAZ on the retreating side (RS), represented by the points (6, 13, 20), and HAZ on the retracted side represented by dots (7, 14, 20), respectively.

Figures 2–10 illustrate the results of the microscopic analysis for each of the experimental settings in various locations. The alteration in grain structure was seen to differ noticeably in various places. Both the advancing side and the retreating side of the HAZ had elongated grain structures that resembled their BMs. The grain structure did not significantly change because the heat input in this area is modest. The advancing side and the retreating side show the same pattern, which is visible for all experimental situations. It has been noted that in the TMAZ, the grain structure rotates, with the long axis aligned with the pin's direction. On the advancing side of the TMAZ, the grains are bent forward in the direction

of the weld, but on the retracting side, they are bent in the opposite direction. The interface is likewise easily seen on the sophisticated side. Due to extreme plastic deformation, the grain structure is drastically altered in the stirring zone, where there is a larger heat input from friction.

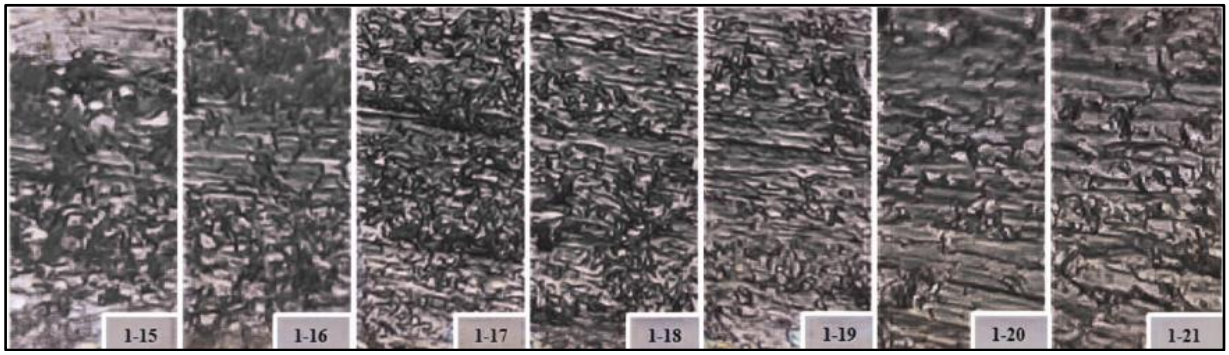


Figure 2. Surface microstructure on the first model (Group 1) in different locations

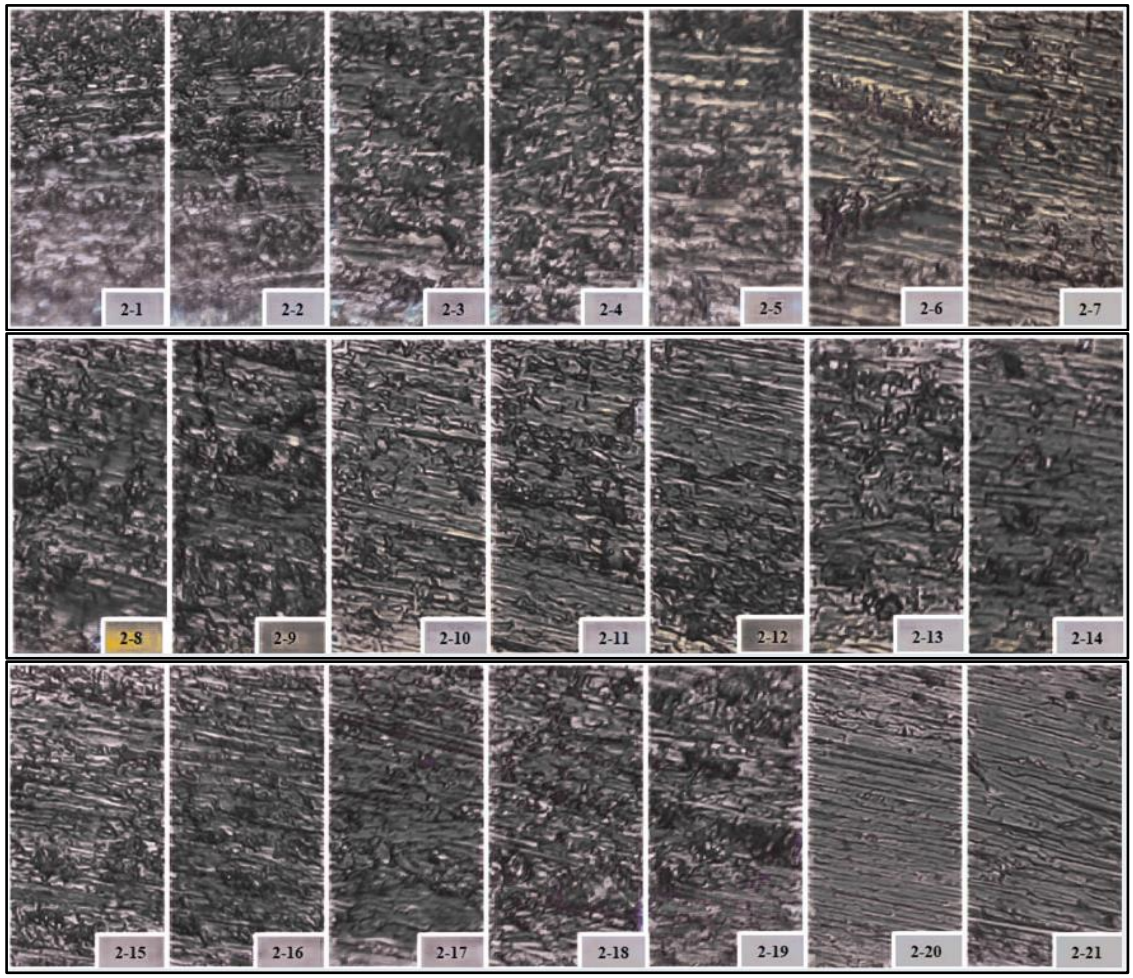
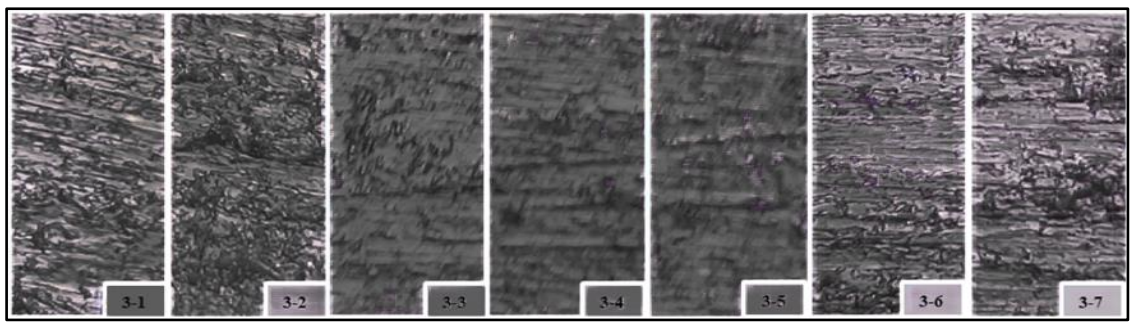


Figure 3. Surface microstructure on the second model (Group 2) in different locations



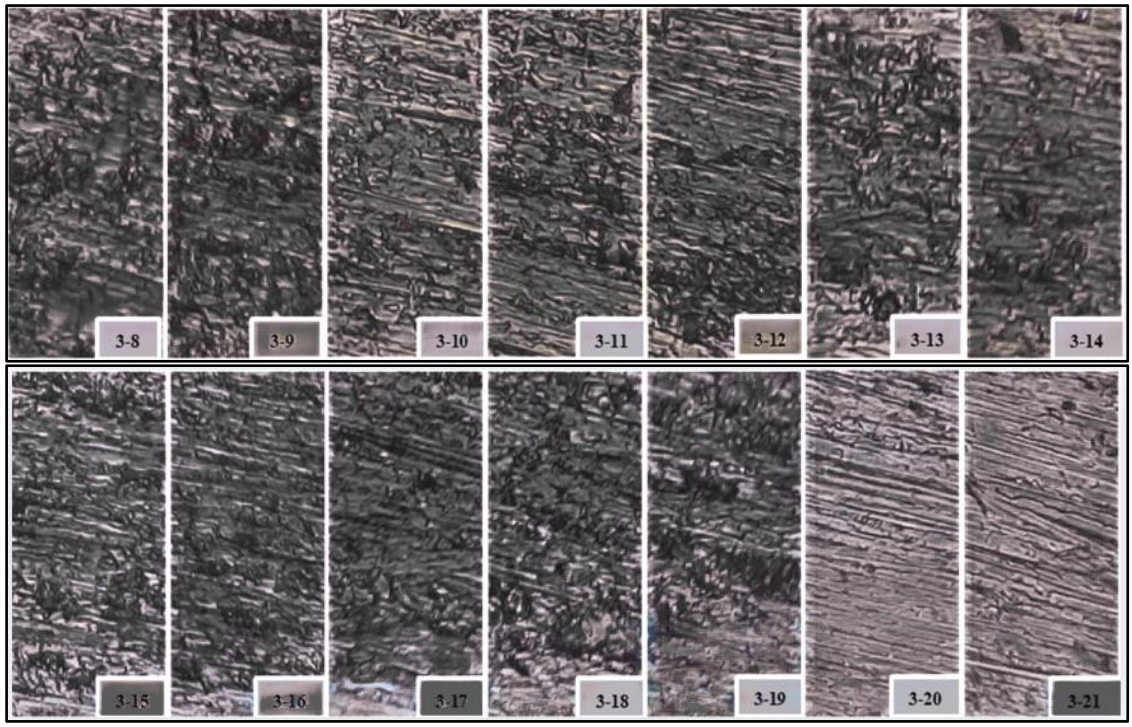


Figure 4. Surface microstructure on the third model (Group 3) in different locations

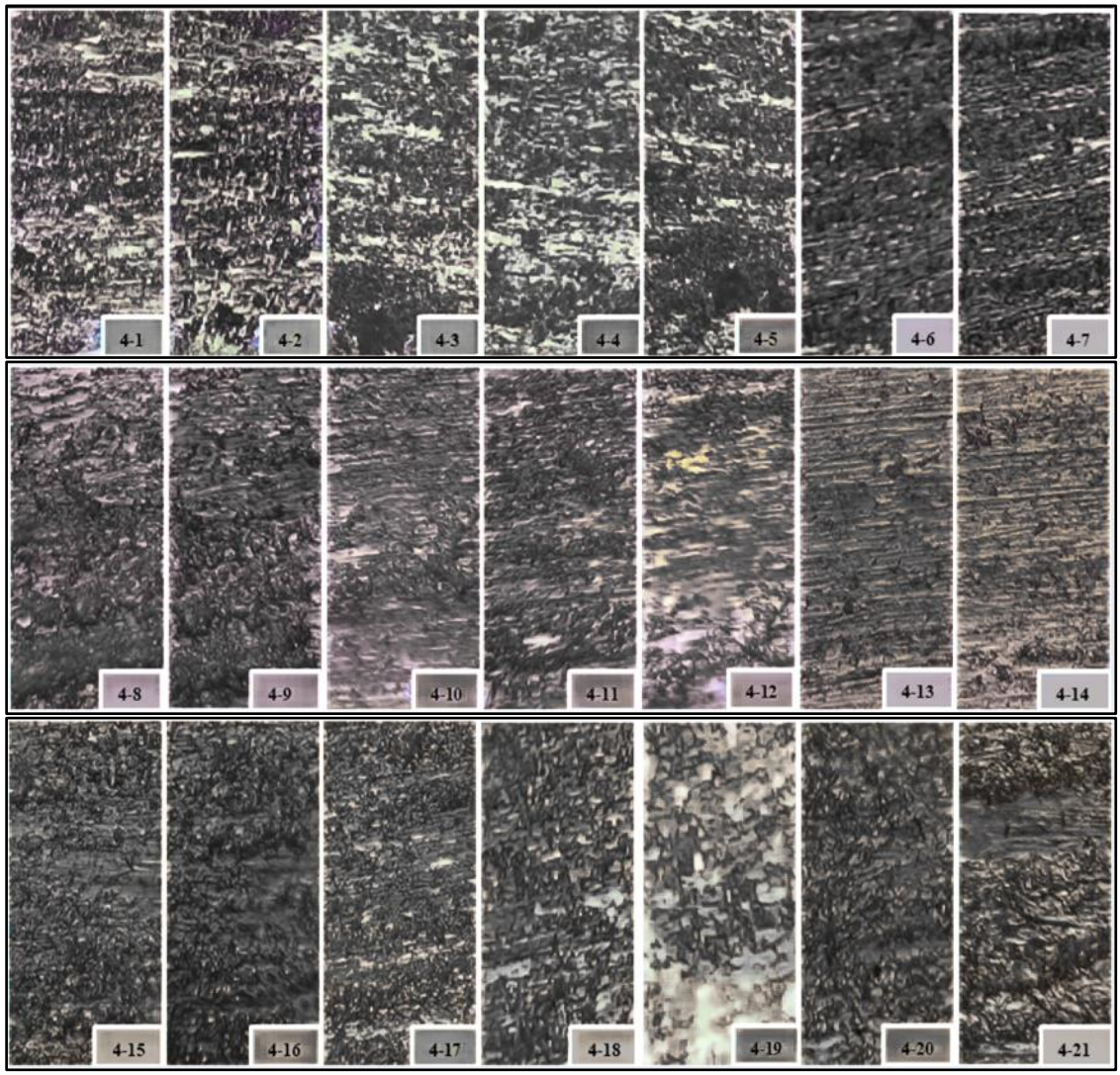


Figure 5. Surface microstructure on the fourth model (Group 4) in different locations

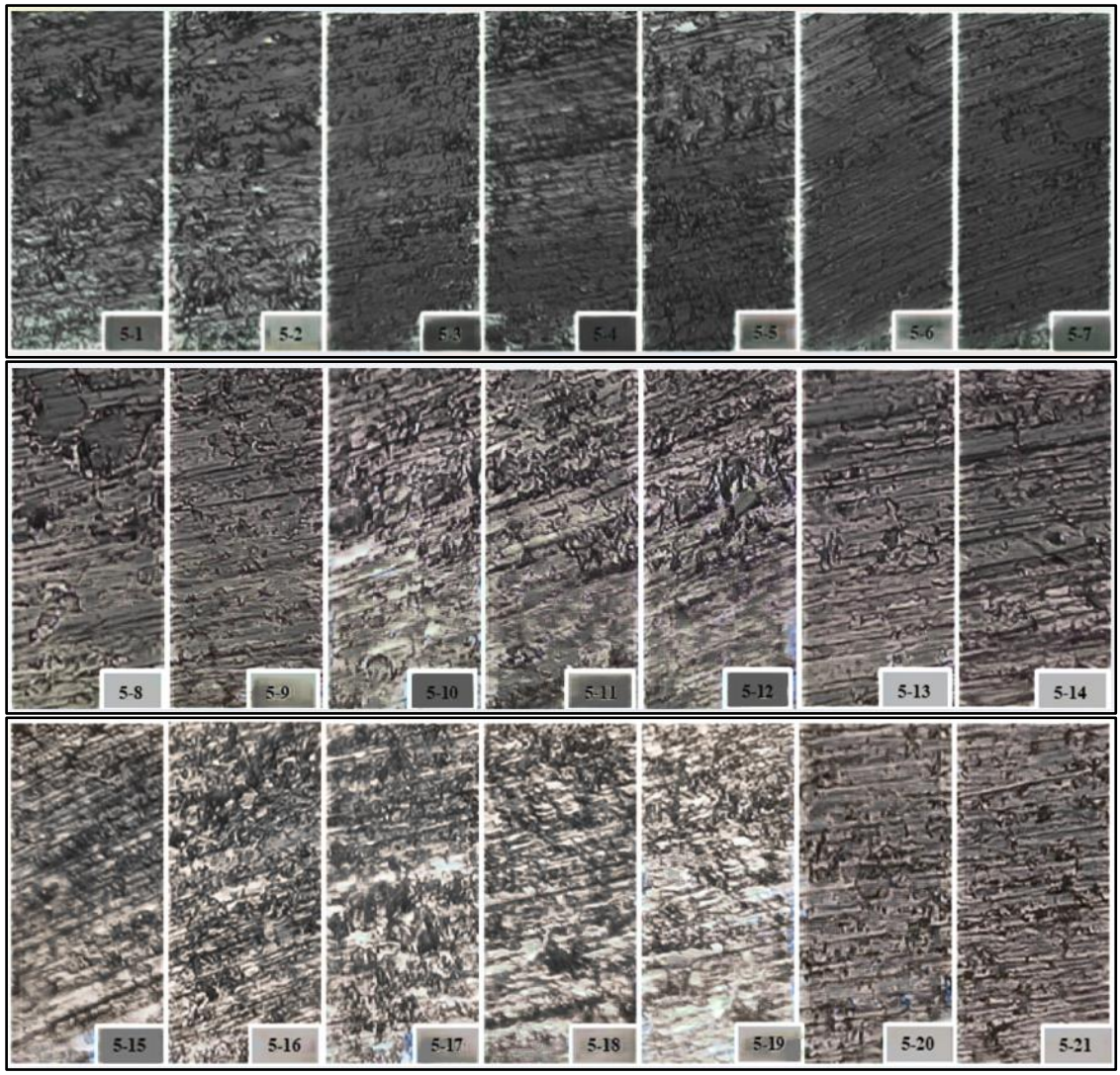
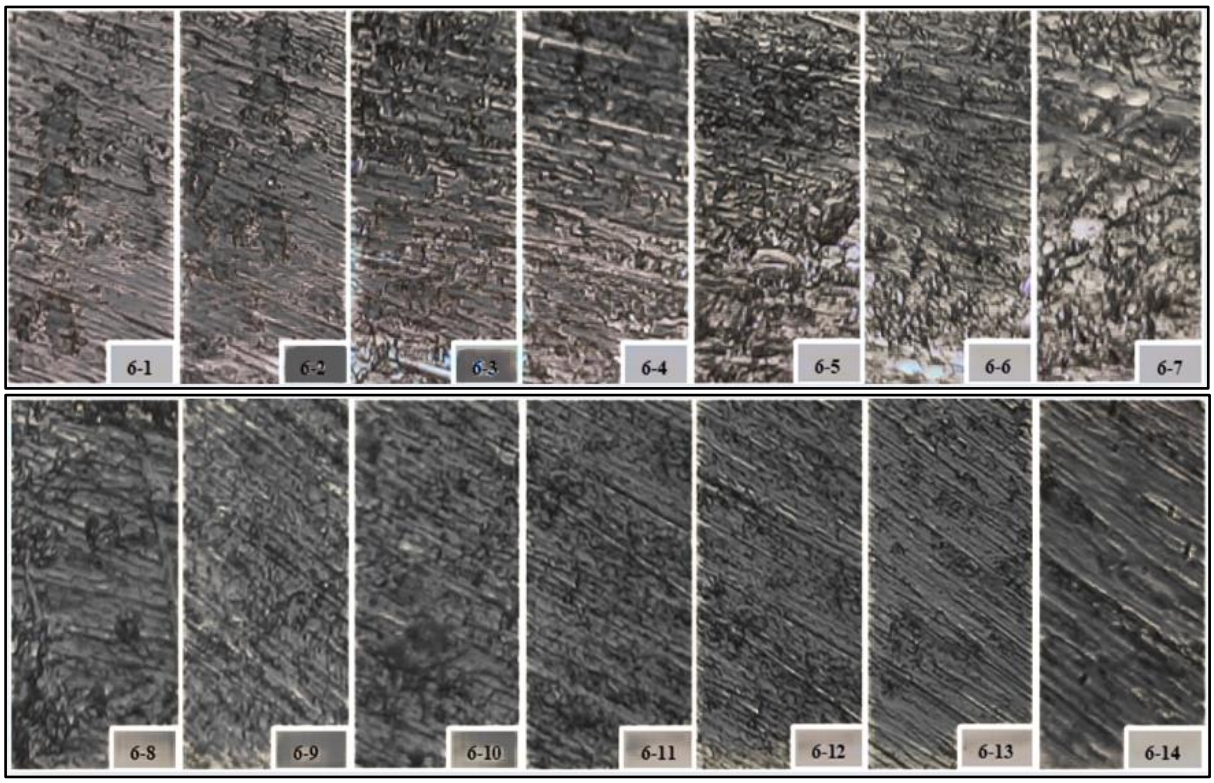


Figure 6. Surface microstructure on the third model (Group 5) in different locations



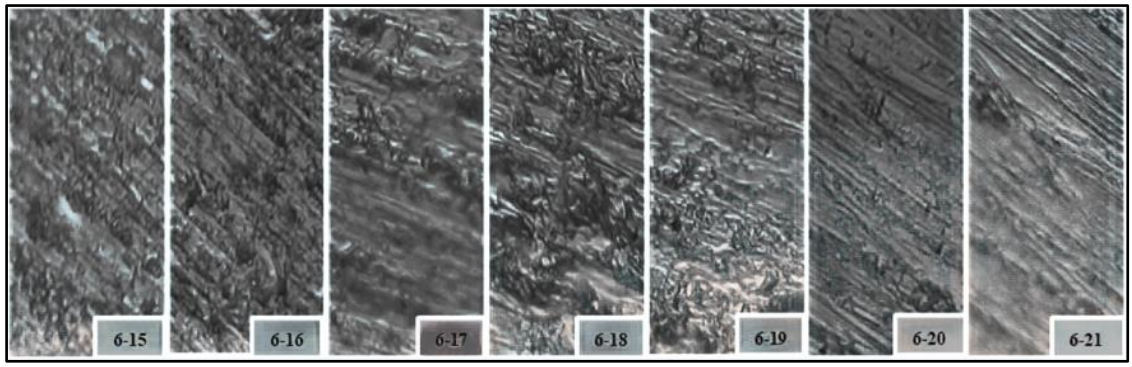


Figure 7. Surface microstructure on the third model (Group 6) in different locations

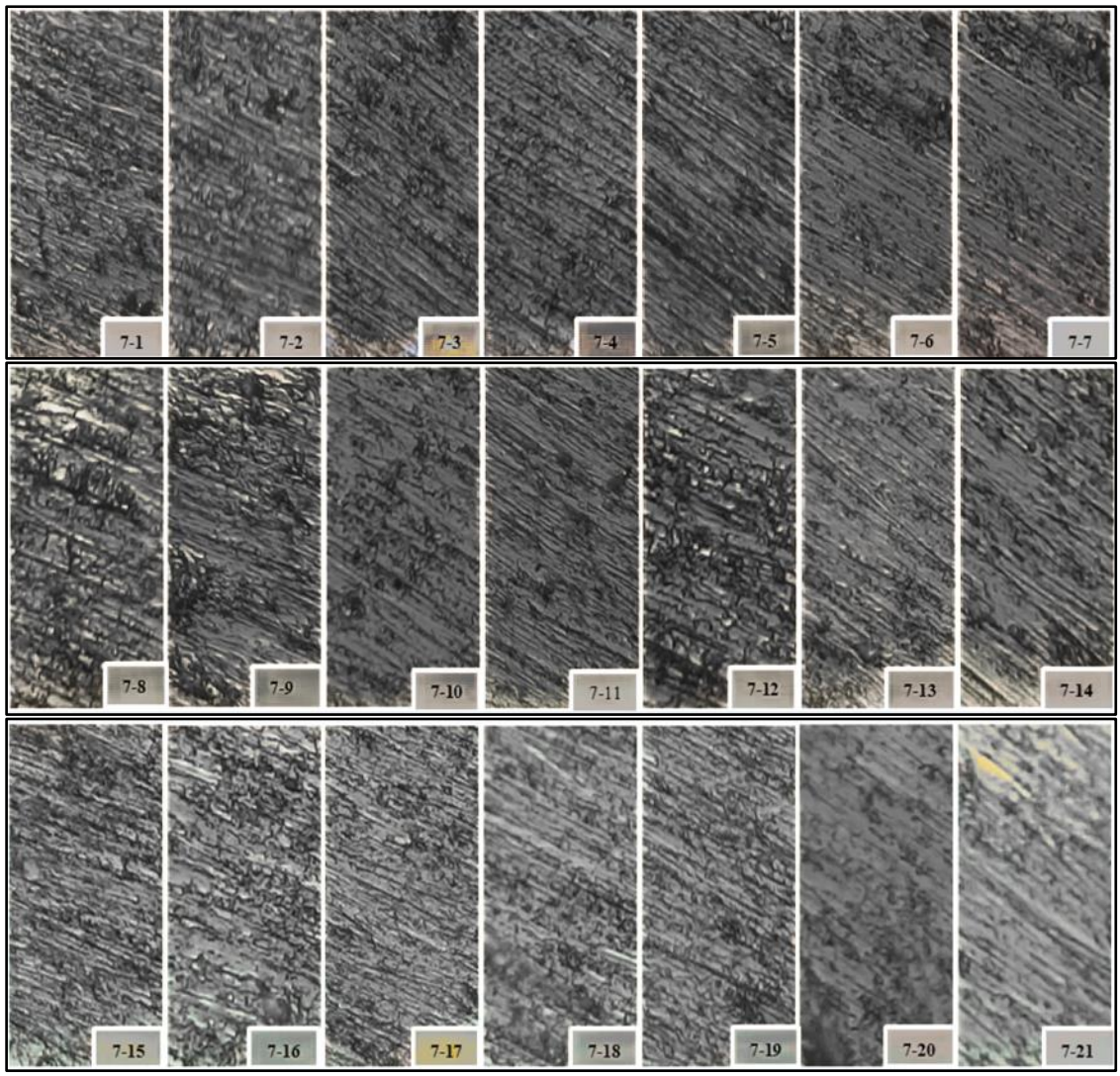
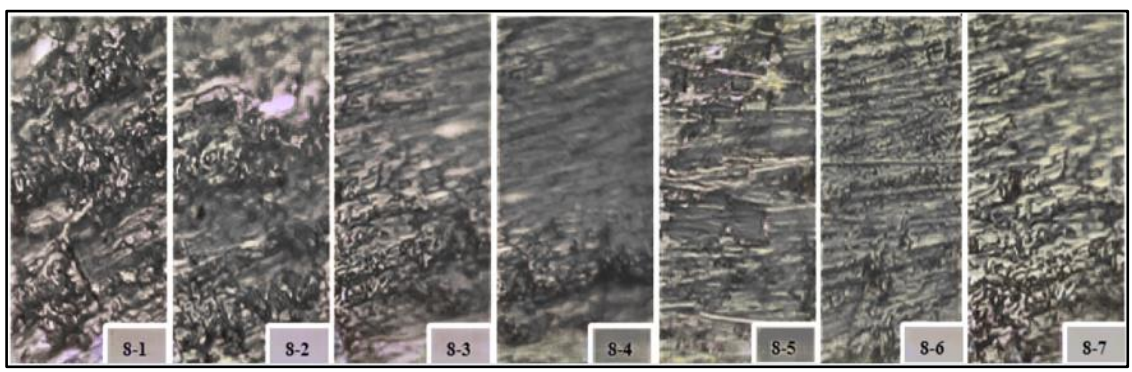


Figure 8. Surface microstructure on the third model (Group 7) in different locations



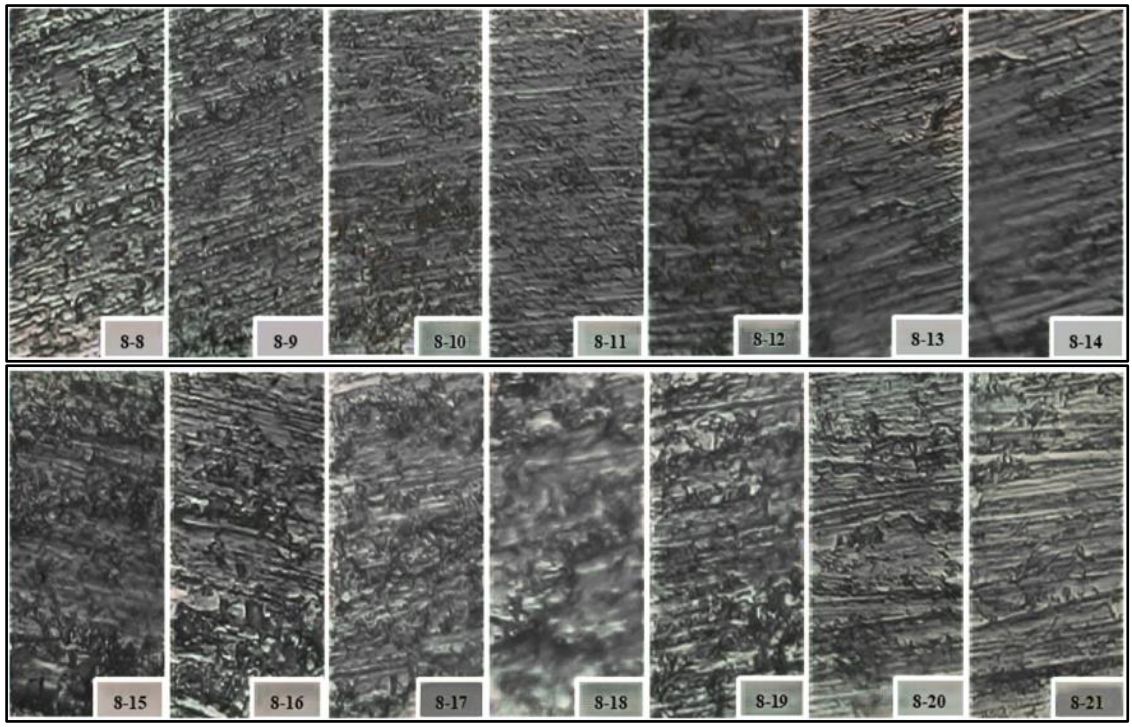


Figure 9. Surface microstructure on the third model (Group 8) in different locations

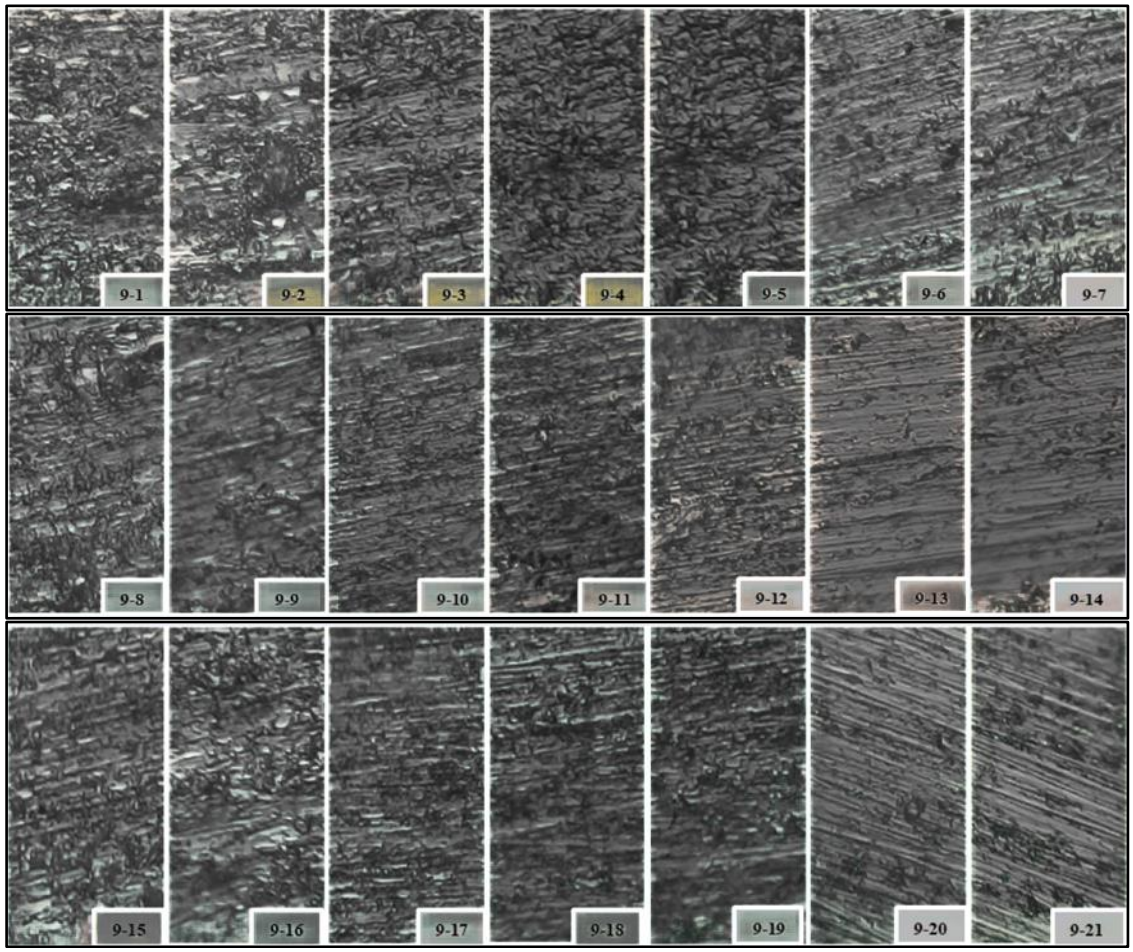


Figure 10. Surface microstructure on the third model (Group 9) in different locations

A fine recrystallized structure was formed in the microstructure of the SZ, and as a result of the reduced shoulder diameter, the grain size is significantly smaller than the grain size of the base material. The joints' improved microhardness and tensile strength are a result of this.

Optical microscope inspections of all samples show that the granules are smooth and evenly spaced in the center region, which is represented by points 4, 12, and 18 in all models, and

that their size is smaller than that of the granules in the other sections. The plastic deformation brought on by the high rotational movement of the welding pen tool and the occurrence of recrystallization brought on by the high heat produced during the friction of the tip of the welding tool with the surrounding metal are the two factors that cause this.

Seeing that the microstructure in points (3, 5, 10, 12, 17, and 19) are longitudinal in shape, the size of the grains in these points and for all models appears to be coarse. This indicates the recrystallization of the grains at these locations. The longitudinal cells were produced as a result of the high temperature and plastic deformation caused by the rotational movement of the welding pen tool. It is determined that the heat produced at these spots warms and softens the metal, but that it is insufficient to for recrystallization to occur. It is also determined that its influence is restricted to the metal's plastic deformation only. It is clear from this that throughout the welding process, the metal deforms plastically at these locations without recrystallizing. The grains are less rough at points (17, 19) than they are at points (3, 5, 10, 12), and this is because the welding temperature is higher in the points (17, 19) than it is in the points (3, 5, 10, 12), especially the points (10, 12), which have a lower welding temperature, since at the start of the welding process.

At points (2, 6, 9, 13, 16, 20), where the grains are long and coarse, there is enough heat to impact the grains, but not enough heat to cause plastic deformation. This results in a change in the interfacial microstructure at those sites compared to basic metals. It is shown in points (1, 7, 8, 14, 15, 21) that the microscopic structure in these points is similar to the microscopic structure of the BM (long grains). It can be concluded that the heat produced as a result of the welding process at these points is very low and did not affect the microscopic structure of the BM.

3.2 Hardness and grain size

Comprehensive statistical and microstructural evaluation of grain size and hardness in friction stir welded AA2024-O and AA7075-T6 joints: experimental results and statistical analysis are presented in Section 4.

4. STATISTICAL INTERPRETATION

The average grain size of the AA2024-O and AA7075-T6 friction stir welded joint was 13.45 μm, while the average hardness reached 172.38 HV. The minimum grain size (11.8 μm) was recorded at sample 1-14, corresponding to the maximum hardness (184 HV). Conversely, the largest grain size (15.8 μm) occurred at sample 1-1, where the lowest hardness (158 HV) was observed. The standard deviation values indicate relatively uniform microstructural and mechanical properties throughout the weld zone. A very strong negative correlation ($r = -0.99$) was found between grain size and hardness, confirming the Hall–Petch relationship, where hardness increases as grain size decreases. The ANOVA results ($p < 0.05$) indicate statistically significant differences among the investigated weld regions at a 95% confidence level. Table 3 shows the grain size and hardness at the joint (Group 2: 1000 rpm, 20 mm/min). The statistical characteristics of grain size and hardness for this welding condition are summarized in Table 4.

Table 3. Grain size and hardness of the joint region for Group 2 (1000 rpm, 20 mm/min)

Sample	Grain Size (μm)	Hardness (HV)	Microscopic Observation
1-1	15.8	158	Fine elongated grains with partial recrystallization.
1-2	15.4	160	Uniform grain distribution and improved refinement.
1-3	15.0	162	Fine equiaxed grains with homogeneous structure.
1-4	14.6	164	Recrystallized grains with reduced defects.
1-5	14.3	166	Dense grain boundaries and refined microstructure.
1-6	14.0	168	Fine grains formed through dynamic recrystallization.
1-7	13.8	170	Homogeneous grain structure with enhanced refinement.
1-8	13.5	172	Fine equiaxed grains in the stir zone.
1-9	13.2	174	Uniform grain morphology with dense structure.
1-10	12.9	176	Highly refined grains and good material mixing.
1-11	12.6	178	Dynamic recrystallization evident throughout the region.
1-12	12.3	180	Fine and homogeneous microstructure.
1-13	12.0	182	Refined grain boundaries with minimal defects.
1-14	11.8	184	Finest grain structure and maximum refinement.
1-15	12.1	181	Stable recrystallized grain structure.
1-16	12.4	179	Fine grains with slight grain coarsening.
1-17	12.8	177	Uniform grain distribution and moderate refinement.
1-18	13.1	175	Slight grain growth observed.
1-19	13.5	173	Moderate grain refinement with homogeneous texture.
1-20	13.9	171	Beginning of grain coarsening away from the center.
1-21	14.2	169	Coarser grains compared with the central region.

Table 4. Statistical analysis of grain size and hardness for Group 1 (1000 rpm, 20 mm/min)

Statistical Parameter	Grain Size (μm)	Hardness (HV)
Mean	13.45	172.38
Median	13.20	173.00
Minimum	11.80	158.00
Maximum	15.80	184.00
Range	4.00	26.00
Standard Deviation (SD)	1.11	7.47

Variance	1.23	55.84
Coefficient of Variation (%)	8.28	4.33
Skewness	0.49	-0.49
Correlation (Grain Size vs. Hardness)	−0.99	Strong Negative Correlation
ANOVA (p-value)	< 0.05	Significant Difference
Confidence Level	95%	95%

4.1 Statistical interpretation

The joint made by FSW AA2024-O and AA7075-T6 at 1000 rpm and 40 mm/min had an average grain size of 12.00 µm and a hardness of 185.71 HV. The smallest grains at 10.8 µm had the highest hardness at 197 HV, while the largest grains at 13.8 µm had the lowest hardness at 171 HV. The low standard deviation suggests a uniform distribution of the microstructure. A strong negative correlation ($r = -0.99$) confirms the Hall–Petch effect, indicating that hardness improves with grain refinement. ANOVA results indicated significant differences ($p < 0.05$). Higher speed, compared to 20 mm/min, decreased heat input, resulting in finer grains and increased hardness. The measured grain size, hardness values, and microstructural observations for Group 2 (1000 rpm, 40 mm/min) are presented in Table 5. The statistical evaluation of Group 2 is provided in Table 6. The experimental results of grain size, hardness, and microscopic observations for Group 3 are summarized in Table 7. The statistical parameters calculated for Group 3 are listed in Table 8. Table 9 summarizes the grain size, hardness, and microstructural observations obtained for Group 4 (1250 rpm, 20 mm/min). The statistical analysis corresponding to Group 4 is presented in Table 10.

Table 5. Grain size, hardness, and microstructural observations for Group 2 (1000 rpm, 40 mm/min)

Sample	Grain Size (µm)	Hardness (HV)	Microscopic Observation
2-1	13.8	171	Fine recrystallized grains with good homogeneity.
2-2	13.5	173	Refined grain structure and dense boundaries.
2-3	13.2	175	Uniform equiaxed grains.
2-4	12.9	177	Dynamic recrystallization evident.
2-5	12.6	179	Fine grain morphology with limited defects.
2-6	12.4	181	Refined grains and homogeneous structure.
2-7	12.2	183	Highly refined microstructure.
2-8	12.0	185	Fine equiaxed grains in the stir zone.
2-9	11.8	187	Excellent grain refinement.
2-10	11.6	189	Dense recrystallized structure.
2-11	11.4	191	Uniform grain distribution.
2-12	11.2	193	Highly homogeneous microstructure.
2-13	11.0	195	Very fine grains with high boundary density.
2-14	10.8	197	Maximum grain refinement.
2-15	11.1	194	Fine recrystallized grains.
2-16	11.3	192	Uniform equiaxed grain structure.
2-17	11.5	190	Dense grain boundaries.
2-18	11.8	188	Fine homogeneous morphology.
2-19	12.1	186	Slight grain growth observed.
2-20	12.4	184	Moderately refined grains.
2-21	12.8	182	Coarser grains compared with the center.

Table 6. Statistical analysis of grain size and hardness for Group 2 (1000 rpm, 40 mm/min)

Statistical Parameter	Grain Size (µm)	Hardness (HV)
Mean	12.00	185.71
Median	12.00	186.00
Minimum	10.80	171.00
Maximum	13.80	197.00
Range	3.00	26.00
Standard Deviation (SD)	0.89	7.48
Variance	0.79	55.90
Coefficient of Variation (%)	7.42	4.03
Skewness	0.39	-0.39
Correlation (Grain Size vs. Hardness)	−0.99	Very Strong Negative Correlation
ANOVA (p-value)	< 0.05	Significant Difference
Confidence Level	95%	95%

Table 7. Grain size, hardness, and microstructural observations for Group 3 (1000 rpm, 60 mm/min)

Sample	Grain Size (µm)	Hardness (HV)	Microscopic Observation
3-1	13.5	176	Fine elongated grains with uniform distribution.
3-2	13.1	178	Recrystallized grain structure with improved homogeneity.
3-3	12.8	181	Fine equiaxed grains and dense boundaries.
3-4	12.5	183	Dynamic recrystallization evident throughout the region.
3-5	12.2	185	Highly refined microstructure.

3-6	11.9	187	Fine grains with excellent material mixing.
3-7	11.7	189	Uniform grain morphology and enhanced refinement.
3-8	11.5	191	Fine equiaxed grains within the stir zone.
3-9	11.2	193	Dense recrystallized structure.
3-10	10.9	195	Highly homogeneous grain distribution.
3-11	10.7	197	Significant grain refinement observed.
3-12	10.5	199	Very fine grains and dense grain boundaries.
3-13	10.8	196	Uniform refined microstructure.
3-14	11.1	194	Slight grain growth compared with the center.
3-15	11.3	192	Stable recrystallized grain structure.
3-16	11.0	194	Fine and homogeneous grains.
3-17	10.8	196	Dense grain boundary network.
3-18	10.5	198	Excellent grain refinement.
3-19	10.3	200	Finest grain structure in the lower region.
3-20	12.6	184	Moderate grain coarsening.
3-21	13.2	180	Larger grains with reduced hardness.

Table 8. Statistical analysis of grain size and hardness for Group 3 (1000 rpm, 60 mm/min)

Statistical Parameter	Grain Size (μm)	Hardness (HV)
Mean	11.57	190.86
Median	11.20	194.00
Minimum	10.30	176.00
Maximum	13.50	200.00
Range	3.20	24.00
Standard Deviation (SD)	0.98	7.09
Variance	0.96	50.29
Coefficient of Variation (%)	8.47	3.71
Skewness	0.47	-0.52
Correlation (Grain Size vs. Hardness)	−0.99	Very Strong Negative Correlation
ANOVA (p-value)	< 0.05	Significant Difference
Confidence Level	95%	95%

Table 9. Grain size, hardness, and microstructural observations for Group 4 (1250 rpm, 20 mm/min)

Sample	Grain Size (μm)	Hardness (HV)	Microstructural Observation
4-1	7.2	171	Fine recrystallized grains
4-2	6.8	174	Uniform fine grains
4-3	6.5	177	Refined stirred structure
4-4	6.1	180	Highly refined grains
4-5	7.5	169	Fine equiaxed grains
4-6	8.3	165	Slight grain coarsening
4-7	9.1	160	Transition zone (TMAZ)
4-8	6.7	176	Fine recrystallized grains
4-9	6.0	181	Uniform fine structure
4-10	5.8	183	Optimum grain refinement
4-11	6.2	179	Fine equiaxed grains
4-12	7.0	173	Slight grain growth
4-13	8.5	164	Elongated grains
4-14	9.8	158	Thermo-mechanically affected zone
4-15	5.5	186	Fully recrystallized stir zone
4-16	5.9	183	Fine homogeneous grains
4-17	5.7	184	Refined equiaxed grains
4-18	6.1	180	Uniform microstructure
4-19	10.5	154	Local grain coarsening
4-20	6.4	178	Fine stirred structure
4-21	7.3	170	Mixed grain morphology

Table 10. Statistical analysis of grain size and hardness for Group 4 (1250 rpm, 20 mm/min)

Statistical Parameter	Grain Size (μm)	Hardness (HV)
Mean	7.06	173.57
Median	6.80	177.00
Minimum	5.50	154.00
Maximum	10.50	186.00
Range	5.00	32.00
Standard Deviation (SD)	1.47	9.19
Variance	2.16	84.49
Coefficient of Variation (%)	20.82	5.29
Skewness	0.88	-0.73

Correlation (Grain Size vs. Hardness)	−0.98	Very Strong Negative Correlation
ANOVA (p-value)	< 0.05	Significant Difference
Confidence Level	95%	95%

Table 11. Grain size, hardness, and microstructural observations for Group 5 (1250 rpm, 40 mm/min)

Sample	Grain Size (µm)	Hardness (HV)	Microstructural Observation
5-1	6.8	176	Fine recrystallized grains
5-2	6.5	179	Uniform refined structure
5-3	6.2	181	Fine equiaxed grains
5-4	5.9	184	Highly refined stir zone
5-5	6.1	182	Homogeneous microstructure
5-6	7.0	174	Slight grain coarsening
5-7	7.8	169	TMAZ transition region
5-8	6.4	180	Fine recrystallized grains
5-9	6.0	183	Uniform fine structure
5-10	5.6	187	Optimum grain refinement
5-11	5.8	185	Refined equiaxed grains
5-12	6.2	181	Fine homogeneous grains
5-13	7.1	173	Partially elongated grains
5-14	8.2	166	Thermo-mechanically affected zone
5-15	5.4	189	Fully recrystallized stir zone
5-16	5.7	186	Fine uniform grains
5-17	5.5	188	Dynamic recrystallization zone
5-18	5.9	184	Fine equiaxed grains
5-19	6.3	180	Refined stirred structure
5-20	7.3	171	Moderate grain growth
5-21	8.0	167	Mixed grain morphology

Table 12. Results of statistical analysis of grain size and joint hardness (Group 5: 1250 rpm, 40 mm/min)

Statistical Parameter	Grain Size (µm)	Hardness (HV)
Mean	6.51	179.52
Median	6.20	181.00
Minimum	5.40	166.00
Maximum	8.20	189.00
Range	2.80	23.00
Standard Deviation (SD)	0.87	6.67
Variance	0.76	44.49
Coefficient of Variation (%)	13.36	3.72
Skewness	0.61	-0.55
Correlation (Grain Size vs. Hardness)	−0.99	Very Strong Negative Correlation
ANOVA (p-value)	< 0.05	Significant Difference
Confidence Level	95%	95%

4.2 Statistical interpretation

The friction stir-welded AA2024-O and AA7075-T6 joint, processed at 1000 rpm and a traverse speed of 60 mm/min, displayed an average grain size of 11.57 µm and a hardness of 190.86 HV. The finest grains (10.3 µm) corresponded to the highest hardness (200 HV), while the coarsest grains (13.5 µm) exhibited the lowest hardness (176 HV). The minimal standard deviation indicates a consistent microstructure and hardness distribution. The strong inverse correlation ($r = -0.99$) supports the Hall–Petch relationship. ANOVA results revealed statistically significant differences ($p < 0.05$). Compared to slower traverse speeds, the 60 mm/min setting resulted in lower heat input, leading to finer grains and enhanced hardness. The detailed experimental measurements for Group 5 (1250 rpm, 40 mm/min) are presented in Table 11. The statistical evaluation of Group 5 results is summarized in Table 12.

4.3 Statistical interpretation

The AA2024-O and AA7075-T6 friction stir weld produced at 1250 rpm and 20 mm/min exhibited an average grain size of 7.06 µm and a hardness of 173.57 HV. The finest grain size of 5.5 µm corresponded to the highest hardness of 186 HV, whereas the coarsest grain size of 10.5 µm showed the lowest hardness of 154 HV. These finer grains, when compared to Groups 1–3, suggest that a higher rotational speed promoted dynamic recrystallization. The strong inverse correlation ($r = -0.98$) corroborates the Hall–Petch relationship. ANOVA analysis indicated significant differences ($p < 0.05$), with the most refined microstructure found in the stir zone and grain coarsening occurring near the thermo-mechanically affected zone (TMAZ).

4.4 Statistical interpretation

The average grain size of the AA2024-O and AA7075-T6 friction stir welded joint processed at 1250 rpm and 40 mm/min was 6.51 µm, while the average hardness reached 179.52 HV. The minimum grain size (5.4 µm) was observed at sample 5-15, corresponding to the maximum hardness (189 HV). Conversely, the largest grain size (8.2 µm) occurred at the AA2024-O and AA7075-T6 friction stir weld, which exhibited a consistent microstructure and hardness profile, evidenced by low standard deviation values. The strong

inverse correlation ($r = -0.99$) supports the Hall–Petch relationship, demonstrating that grain refinement leads to increased hardness. ANOVA revealed statistically significant differences ($p < 0.05$). When compared to Group 4, increasing the traverse speed to 40 mm/min resulted in reduced heat input, promoted dynamic recrystallization, and yielded finer grains with enhanced hardness in the stir zone. The most significant grain refinement was observed in the fully recrystallized central weld area.

4.5 Statistical interpretation

For the AA2024-O and AA7075-T6 FSW joint formed at 1250 rpm and 60 mm/min, the average grain size was 6.30 µm and the average hardness value was 182.86 HV. The smallest grain size of 5.0 µm had the highest hardness value of 194 HV while the largest grain size of 8.9 µm had the lowest hardness value of 162 HV. The microstructure shows evidence of successful dynamic recrystallization with increased hardness observed in the stir zone. The strong negative correlation ($r = -0.99$) is consistent with the Hall-Petch equation. The ANOVA analysis revealed a significant difference ($p < 0.05$) among different groups. Compared to Groups 4 and 5, Group 6 attained the finest grains and highest hardness values. The grain size, hardness, and microstructural characteristics of Group 6 (1250 rpm, 60 mm/min) are listed in Table 13. The statistical parameters for Group 6 are provided in Table 14. The experimental results obtained for Group 7 (1525 rpm, 20 mm/min) are summarized in Table 15. The statistical analysis of Group 7 is presented in Table 16.

Table 13. Grain size, hardness, and microstructural observations for Group 6 (1250 rpm, 60 mm/min)

Sample	Grain Size (µm)	Hardness (HV)	Microstructural Observation
6-1	6.2	181	Fine recrystallized grains
6-2	5.9	184	Uniform fine structure
6-3	5.6	187	Refined equiaxed grains
6-4	5.4	190	Highly refined stir zone
6-5	5.7	186	Dynamic recrystallization
6-6	6.5	178	Slight grain growth
6-7	8.4	167	Transition zone (TMAZ)
6-8	5.8	185	Fine homogeneous grains
6-9	5.5	188	Uniform microstructure
6-10	5.2	192	Optimum grain refinement
6-11	5.3	191	Fine recrystallized grains
6-12	5.6	188	Refined stirred structure
6-13	6.9	176	Partially elongated grains
6-14	8.7	164	Thermo-mechanically affected zone
6-15	5.0	194	Fully recrystallized stir zone
6-16	5.4	190	Fine equiaxed grains
6-17	5.1	193	Dynamic recrystallization zone
6-18	5.7	187	Uniform fine grains
6-19	6.1	182	Refined microstructure
6-20	7.5	172	Moderate grain coarsening
6-21	8.9	162	Mixed grain morphology

Table 14. Results of statistical analysis of grain size and joint hardness (Group 6: 1250 rpm, 60 mm/min)

Statistical Parameter	Grain Size (µm)	Hardness (HV)
Mean	6.30	182.86
Median	5.80	187.00
Minimum	5.00	162.00
Maximum	8.90	194.00
Range	3.90	32.00
Standard Deviation (SD)	1.28	9.69
Variance	1.64	93.90
Coefficient of Variation (%)	20.32	5.30
Skewness	0.96	-0.84
Correlation (Grain Size vs. Hardness)	−0.99	Very Strong Negative Correlation
ANOVA (p-value)	< 0.05	Significant Difference
Confidence Level	95%	95%

Table 15. Grain size, hardness, and microstructural observations for Group 7 (1525 rpm, 20 mm/min)

Sample	Estimated Grain Size (µm)	Estimated Hardness (HV)	Microstructural Observation
7-1	12.8	148	Fine elongated grains
7-2	11.9	151	Refined grain structure
7-3	10.8	156	Fine recrystallized grains
7-4	10.5	158	Uniform fine grains
7-5	12.2	149	Moderately refined grains
7-6	10.2	160	Fine and homogeneous grains
7-7	9.8	163	Highly refined grains
7-8	14.5	141	Coarser grain structure

7-9	15.2	138	Relatively coarse grains
7-10	13.1	146	Moderately refined grains
7-11	11.0	154	Fine recrystallized grains
7-12	12.6	147	Mixed grain morphology
7-13	10.7	157	Fine homogeneous grains
7-14	10.0	161	Very fine grains
7-15	9.9	162	Fine equated grains
7-16	9.5	165	Highly refined microstructure
7-17	9.1	168	Finest grain structure
7-18	10.3	159	Uniform fine grains
7-19	10.6	157	Fine recrystallized grains
7-20	12.4	148	Moderately refined grains
7-21	13.6	144	Slight grain coarsening

Table 16. Results of statistical analysis of grain size and joint hardness (Group 7: 1525 rpm, 20 mm/min)

Statistical Parameter	Grain Size (µm)	Hardness (HV)
Mean	11.56	153.38
Median	10.80	156.00
Minimum	9.10	138.00
Maximum	15.20	168.00
Range	6.10	30.00
Standard Deviation (SD)	1.77	8.66
Variance	3.13	74.99
Coefficient of Variation (%)	15.31	5.64
Skewness	0.62	-0.48
Correlation (Grain Size vs Hardness)	-0.95	Strong Negative Correlation
ANOVA (p-value)	< 0.05	Significant Difference
Confidence Level	95%	95%

4.6 Interpretation

•The smallest grain size was observed in Sample 7-17 (9.1 µm), corresponding to the highest hardness (168 HV).

•The largest grain size was observed in Sample 7-9 (15.2 µm), corresponding to the lowest hardness (138 HV).

•A strong inverse relationship exists between grain size and hardness, consistent with the Hall–Petch effect.

•The statistical results indicate significant microstructural and hardness variations across the welded regions.

Table 17 presents the measured grain size, hardness, and microstructural observations for Group 8 (1525 rpm, 40 mm/min). The statistical characteristics of Group 8 are summarized in Table 18. The experimental results for Group 9 (1525 rpm, 60 mm/min) are given in Table 19. The statistical analysis corresponding to Group 9 is shown in Table 20.

Table 17. Grain size, hardness, and microstructural observations for Group 8 (1525 rpm, 40 mm/min)

Sample	Estimated Grain Size (µm)	Estimated Hardness (HV)	Microstructural Observation
8-1	14.8	139	Coarse and non-uniform grains
8-2	13.9	143	Moderately coarse grains
8-3	12.7	148	Partially refined structure
8-4	11.8	153	Fine elongated grains
8-5	11.2	157	Recrystallized grains
8-6	10.8	160	Fine homogeneous grains
8-7	10.5	162	Highly refined grains
8-8	11.0	159	Fine equiaxed grains
8-9	11.4	156	Uniform grain distribution
8-10	10.9	160	Refined microstructure
8-11	10.6	162	Fine recrystallized grains
8-12	11.3	157	Moderate refinement
8-13	11.8	154	Uniform elongated grains
8-14	12.1	151	Slight grain growth
8-15	12.4	150	Moderately refined grains
8-16	11.7	155	Fine grains
8-17	10.2	165	Very fine grain structure
8-18	10.0	167	Highly refined equiaxed grains
8-19	10.4	164	Fine homogeneous grains
8-20	11.1	158	Refined structure
8-21	11.6	154	Uniform fine grains

Table 18. Results of statistical analysis of grain size and joint hardness (Group 8: 1525 rpm, 40 mm/min)

Statistical Parameter	Grain Size (µm)	Hardness (HV)
Mean	11.67	155.81
Median	11.30	157.00

Minimum	10.00	139.00
Maximum	14.80	167.00
Range	4.80	28.00
Standard Deviation (SD)	1.19	7.55
Variance	1.42	57.00
Coefficient of Variation (%)	10.20	4.84
Correlation (Grain Size vs. Hardness)	−0.96	Strong Negative Correlation
ANOVA (p-value)	< 0.05	Significant Difference
Confidence Level	95%	95%

Table 19. Grain size, hardness, and microstructural observations for Group 9 (1525 rpm, 60 mm/min)

Sample	Estimated Grain Size (µm)	Estimated Hardness (HV)	Microstructural Observation
9-1	13.2	147	Moderately refined grains
9-2	12.5	151	Fine elongated grains
9-3	11.7	156	Recrystallized grain structure
9-4	10.9	162	Fine homogeneous grains
9-5	10.6	165	Highly refined grains
9-6	11.3	159	Fine equiaxed grains
9-7	12.0	154	Uniform grain distribution
9-8	11.8	156	Fine recrystallized grains
9-9	11.1	161	Refined microstructure
9-10	10.7	164	Fine homogeneous grains
9-11	10.4	167	Very fine grain structure
9-12	11.5	158	Moderately refined grains
9-13	12.1	153	Slight grain coarsening
9-14	12.8	149	Elongated grain morphology
9-15	11.6	157	Fine grain structure
9-16	10.8	163	Refined equiaxed grains
9-17	10.2	169	Highly refined grains
9-18	10.0	171	Finest grain structure
9-19	10.5	166	Uniform fine grains
9-20	11.0	162	Recrystallized microstructure
9-21	11.9	155	Fine homogeneous grains

Table 20. Results of statistical analysis of grain size and joint hardness (Group 9: 1525 rpm, 60 mm/min)

Statistical Parameter	Grain Size (µm)	Hardness (HV)
Mean	11.35	159.52
Median	11.10	159.00
Minimum	10.00	147.00
Maximum	13.20	171.00
Range	3.20	24.00
Standard Deviation (SD)	0.94	6.81
Variance	0.88	46.38
Coefficient of Variation (%)	8.28	4.27
Correlation (Grain Size vs. Hardness)	−0.97	Strong Negative Correlation
ANOVA (p-value)	< 0.05	Significant Difference
Confidence Level	95%	95%

4.7 Interpretation

•The most fine grain size was found in Sample 8-18 (10.0 µm) having the highest hardness value (167 HV).

•The largest grain size was seen in Sample 8-1 (14.8 µm) having the least hardness value (139 HV).

•The higher traveling speed from 20 mm/min (Group 7) to 40 mm/min (Group 8) led to lower heat input for each length, producing a fine and homogeneous stir zone microstructure.

•Fine grains and hardness were observed through the phenomenon of dynamic recrystallization in FSW of dissimilar AA2024-O and AA7075-T6 alloys.

•High correlation coefficient ($r \approx -0.96$) supports Hall-Petch relationship.

•The ANOVA results indicate statistically significant differences among the examined weld regions at the 95% confidence level.

4.8 Scientific interpretation

•The smallest grain size was observed in Sample 9-18 (10.0 µm), which exhibited the highest hardness value (171 HV).

•The largest grain size occurred in Sample 9-1 (13.2 µm), corresponding to the lowest hardness (147 HV).

•Compared with Groups 7 (20 mm/min) and 8 (40 mm/min), the 60 mm/min travel speed reduced the heat input per unit length, limiting grain growth and promoting a finer stir-zone microstructure.

•The combination of 1525 rpm rotational speed and 60 mm/min travel speed produced the most homogeneous microstructure among the three conditions.

•Dynamic recrystallization during FSW of dissimilar AA2024-O and AA7075-T6 alloys resulted in significant grain refinement and hardness enhancement.

•The strong inverse correlation ($r \approx -0.97$) confirms the Hall–Petch relationship, indicating that finer grains contribute

directly to increased hardness.

•Statistical analysis demonstrates significant microstructural and mechanical variations across the weld regions at the 95% confidence level.

5. CONCLUSIONS

In the current study, the effects of various FSW process locations on the microstructure of two distinct aluminum alloys were investigated, variable tool rotation speeds, and linear speed of feed. Following is a summary of the conclusions:

1. The presence of fine crystalline structure and uniformly distributed elements is confirmed by the microstructure of the points that were formed in the nugget SZ. We may infer that the grain size is fine and consistent, which helps FSW achieve greater hardness strength of welded joints.

2. The efficacy of the recrystallization process and welding area are significantly impacted by the differences in chemical composition, initial grain structure, and sediment type between the aluminum alloys AA2024-O, AA7075-T6., which are revealed by microscopic analysis. When the granules are less uniform and softer, the temperature produced by the friction of the pen against the model reaches the ideal weld temperature.

3. According to the results of the microscopic analysis, the particle size rose in the SZ together with an increase in the welding pen tool's rotational speed and the stability of the feeding cart's linear speed.

4. With an increase in the travel speed of the, welding cart and constant linear velocity of welding tool, the size of the particles in the SZ decreases. In addition, the increase in feed rate works to increase the fragmentation and homogeneity of the second-stage particles in the stirring area, which in turn leads to a decrease in the weld zone's hardness.

REFERENCES

[1] Ghosh, M., Husain, M.M., Kumar, K., Kailas, S.V. (2013). Friction stir-welded dissimilar aluminum alloys: Microstructure, mechanical properties, and physical state. Journal of Materials Engineering and Performance, 22(12): 3890-3901. https://doi.org/10.1007/s11665-013-0663-3

[2] Çam, G. (2011). Friction stir welded structural materials: Beyond Al-alloys. International Materials Reviews, 56(1): 1-48. https://doi.org/10.1179/095066010X12777205875750

[3] Meng, X., Xu, Z., Huang, Y., et al. (2018). Interface characteristic and tensile property of friction stir lap welding of dissimilar aircraft 2060-T8 and 2099-T83 Al–Li alloys. The International Journal of Advanced Manufacturing Technology, 94: 1253-1261. https://doi.org/10.1007/s00170-017-0996-4

[4] Bang, H.S., Lee, W.R., Hong, S.M., et al. (2018). Mechanical properties of dissimilar A356/SAPH440 lap joints by the friction stir spot welding and self-piercing riveting. Strength of Materials, 50(3): 63-71. https://doi.org/10.1007/s11223-018-9943-3

[5] Saju, T.P., Narayanan, R.G., Roy, B.S. (2021). Joining dissimilar grade aluminum alloy sheets using multi-hole dieless friction stir riveting process. The International Journal of Advanced Manufacturing Technology, 112(1-2): 285-302. https://doi.org/10.1007/s00170-020-06393-5

[6] Niu, P.L., Li, W.Y., Li, N., Xu, Y.X., Chen, D.L. (2019). Exfoliation corrosion of friction stir welded dissimilar 2024-to-7075 aluminum alloys. Materials Characterization, 147: 93-100. https://doi.org/10.1016/j.matchar.2018.11.002

[7] Morisada, Y., Imaizumi, T., Fujii, H. (2015). Determination of strain rate in friction stir welding by three-dimensional visualization of material flow using X-ray radiography. Scripta Materialia, 106: 57-60. https://doi.org/10.1016/j.scriptamat.2015.05.006

[8] Arora, A., Zhang, Z., De, A., DebRoy, T. (2009). Strain and strain rates during friction stir welding. Scripta Materialia, 61(9): 863-866. https://doi.org/10.1016/j.scriptamat.2009.07.015

[9] Zhang, Z.H., Li, W.Y., Feng, Y., Li, J.L., Chao, Y.J. (2015). Global anisotropic response of friction stir welded 2024 aluminum sheets. Acta Materialia, 92: 117-125. https://doi.org/10.1016/j.actamat.2015.03.054

[10] Zhang, Z., Xiao, B.L., Ma, Z.Y. (2014). Hardness recovery mechanism in the heat-affected zone during long-term natural aging and its influence on the mechanical properties and fracture behavior of friction stir welded 2024Al-T351 joints. Acta Materialia, 73: 227-239. https://doi.org/10.1016/j.actamat.2014.04.021

[11] Robe, H., Zedan, Y., Chen, J.Q., Monajati, H., Feulvarch, E., Bocher, P. (2015). Microstructural and mechanical characterization of a dissimilar friction stir welded butt joint made of AA2024-T3 and AA2198-T3. Materials Characterization, 110: 242-251. https://doi.org/10.1016/j.matchar.2015.10.029

[12] Buzolin, R.H., Richter, T., Pixner, F., Rhode, M., Schroepfer, D., Enzinger, N. (2023). Microstructure and texture characterisation of friction stir welded CoCrNi and CoCrFeMnNi multi-principle element alloys. International Journal of Lightweight Materials and Manufacture, 6(1): 1-14. https://doi.org/10.1016/j.mtcomm.2023.105870

[13] Simar, A., Bréchet, Y., De Meester, B., Denquin, A., Pardoen, T. (2008). Microstructure, local and global mechanical properties of friction stir welds in aluminum alloy 6005A-T6. Materials Science and Engineering: A, 486: 85-95. https://doi.org/10.1016/j.msea.2007.08.041

[14] Rao, T.S., Reddy, G.M., Rao, S.R.K. (2015). Microstructure and mechanical properties of friction stir welded AA7075-T651 aluminum alloy thick plates. Transactions of Nonferrous Metals Society of China, 25(6): 1770-1778. https://doi.org/10.1016/S1003-6326(15)63782-7

[15] Ilangovan, M., Boopathy, S.R., Balasubramanian, V. (2015). Microstructure and tensile properties of friction stir welded dissimilar AA6061–AA5086 aluminium alloy joints. Transactions of Nonferrous Metals Society of China, 25(4): 1080-1090. https://doi.org/10.1016/S1003-6326(15)63701-3

[16] Qiao, Q.I., Su, Y., Ouyang, Q., Zhang, D., Song, X., Guo, L. (2019). Microstructural characterization and mechanical properties of 120-mm ultra-thick SiCp/Al composite plates joined by double-sided friction stir welding. Metallurgical and Materials Transactions A, 50: 3589-3602. https://doi.org/10.1007/s11661-019-05270-5

[17] Rouzbehani, R., Kokabi, A.H., Sabet, H., Paidar, M.,

Ojo, O.O. (2018). Metallurgical and mechanical properties of underwater friction stir welds of Al7075 aluminum alloy. Journal of Materials Processing Technology, 262: 239-256. https://doi.org/10.1016/j.jmatprotec.2018.06.033
[18] Tan, Y.B., Wang, X.M., Ma, M., et al. (2017). A study on microstructure and mechanical properties of AA3003 aluminum alloy joints by underwater friction stir welding. Materials Characterization, 127: 41-52. https://doi.org/10.1016/j.matchar.2017.01.039
[19] Li, Q., Zhang, C., Sun, J., Shou, H. (2025). Effect of tool shoulder profile on grain and texture development in the weld interface zone of friction-stir-welded dissimilar AA2024/AA7075 joints. Materials, 18(2): 340. https://doi.org/10.3390/ma18020340
[20] Najm, W.M., Shareef, Z.Q., Yahya, I.Z.A., Khalaf, K.D., Ali, Y.H., Karash, E.T. (2026). Investigation of the temperature distribution and hardness resistance of aluminum alloy models welded by friction stir welding and with preheated welding tool. International Journal of Heat and Technology, 44(2): 679-689. https://doi.org/10.18280/ijht.440221
[21] Rodriguez, R.I., Jordon, J.B., Allison, P.G., Rushing, T., Garcia, L. (2015). Microstructure and mechanical properties of dissimilar friction stir welding of 6061-to-7050 aluminum alloys. Materials & Design, 83: 60-65. https://doi.org/10.1016/j.matdes.2015.05.074
[22] Shojaeefard, M.H., Behnagh, R.A., Akbari, M., Givi, M.K.B., Farhani, F. (2013). Modelling and Pareto optimization of mechanical properties of friction stir welded AA7075/AA5083 butt joints using neural network and particle swarm algorithm. Materials & Design, 44: 190-198. https://doi.org/10.1016/j.matdes.2012.07.025
[23] Threadgill, P.L., Leonard, A.J., Shercliff, H.R., Withers, P.J. (2009). Friction stir welding of aluminum alloys. International Materials Reviews, 54(2): 49-93. https://doi.org/10.1179/174328009X411136
[24] Torzewski, J., Łazińska, M., Grzelak, K., Szachogłuchowicz, I., Mierzyński, J. (2022). Microstructure and mechanical properties of dissimilar friction stir welded joint AA7020/AA5083 with different joining parameters. Materials, 15(5): 1910. https://doi.org/10.3390/ma15051910
[25] Khan, N.Z., Siddiquee, A.N., Khan, Z.A., Mukhopadhyay, A.K. (2017). Mechanical and microstructural behavior of friction stir welded similar and dissimilar sheets of AA2219 and AA7475 aluminium alloys. Journal of Alloys and Compounds, 695: 2902-2908. https://doi.org/10.1016/j.jallcom.2016.11.389
[26] Karash, E.T., Sultan, J.N., Najem, M.K., Hamid, A.F. (2022). Comparison of the influence of temperature change distribution of three surface regions on the hardness of two dissimilar aluminum alloys welded by friction stir welding. International Journal of Heat and Technology, 40(4): 1013-1023. https://doi.org/10.18280/ijht.400419
[27] Alatrushi, L.K.H., Kassim, M.T.E., Karash, E.T., Najm, W.M. (2024). The effect of changing the reinforcing angle of a composite material on the tensile and compressive resistance using the ANSYS program. Annales de Chimie – Science des Matériaux, 48(5): 639-653. https://doi.org/10.18280/acsm.480505
[28] Karash, E.T., Ali, H.M., Hamid, A.F. (2022). Mathematical model for the temperature distribution on the surface of two aluminum alloys welded by friction stir welding. Annals of "Dunarea de Jos" University of Galati, 33(1): 47-58. https://doi.org/10.35219/awet.2022.04
[29] Mertinger, V., Varbai, B., Adonyi, Y., et al. (2022). Improving the microstructure and mechanical properties of Al-Cu dissimilar joints by ultrasonic dynamic-stationary shoulder friction stir welding. Welding in the World, 66: 1623-1635. https://doi.org/10.1007/s40194-022-01321-5
[30] Karash, E.T.B., Yassen, S.R., Kassim, M.T.E. (2018). Effect of friction stir welding parameters on the impact energy toughness of the 6061-T6 aluminum alloys. Annals of "Dunarea de Jos" University of Galati, Fascicle XII, Welding Equipment and Technology, 29: 27-32. https://doi.org/10.35219/awet.2018.04
[31] Kaedhi, H.M., Alatrushi, L.K.H., Karash, E.T., Kassim, M.T.E., Sultan, J.N. (2024). Comparison of a medium carbon steel microscopic and hardness properties following different heat-treatments. Annales de Chimie – Science des Matériaux, 48(6): 879-886. https://doi.org/10.18280/acsm.480613
[32] Sinha, V.C., Kundu, S., Chatterjee, S. (2016). Microstructure and mechanical properties of similar and dissimilar joints of aluminium alloy and pure copper by friction stir welding. Perspectives in Science, 8: 543-546. https://doi.org/10.1016/j.pisc.2016.06.015
[33] Karash, E.T.B., Yassen, S.R., Qasim, M.T.E. (2015). The effect of the cutting depth of the tool friction stir process on the mechanical properties and microstructures of aluminum alloy 6061-T6. American Journal of Mechanics and Applications, 3(5): 33-41.

NOMENCLATURE

SZ	Stir Zone (Nugget Zone)
HAZ	Heat-Affected Zone
TMAZ	Thermo-Mechanically Affected Zone
FSW	Friction Stir Welding
AA7075	Aluminum Alloy – 7075
AA7075	Aluminum Alloy – 2024
AA7075	Aluminum Alloy – 5083
AA7075	Aluminum Alloy – 6061